Model-Based Retrieval of Forest Parameters From Sentinel-1 Coherence and Backscatter Time Series

M. Lavalle, C. Telli, N. Pierdicca, *Senior Member, IEEE*, U. Khati, *Member, IEEE*, O. Cartus, and J. Kellndorfer, *Senior Member, IEEE*

***Abstract*— This letter describes a model-based algorithm for estimating tree height and other bio-physical land parameters from time series of synthetic aperture radar (SAR) interferometric coherence and backscatter supported by sparse lidar data. The random-motion-over-ground model (RMoG) is extended to time series and revisited to capture the short- and long-term temporal coherence variability caused by motion of the scatterers and changes in the soil and canopy backscatter. The proposed retrieval algorithm estimates first the spatially slow-varying RMoG model parameters using sparse lidar data, and subsequently the spatially fast-varying model parameters such as tree height. The recently published global Sentinel-1 (S-1) interferometric coherence and backscatter data set and sparse spaceborne GEDI lidar data are used to illustrate the algorithm. Results obtained for a small region over Spain show that the temporal coherence and backscatter time series have the potential to be used for global, model-based land parameter estimation.**

***Index Terms*— Forestry, radar interferometry, synthetic aperture radar (SAR).**

I. Introduction

SEVERAL current and forthcoming synthetic aperture radar (SAR) missions are designed to acquire global data from a narrow orbital tube, effectively delivering dense time series of polarimetric-interferometric *temporal* coherence. Examples of such missions are the C-band Sentinel-1 (S-1), the L- and S-band NASA-ISRO (NISAR), and the L-band ROSE-L, which will provide multiyear coherence and backscatter time series with weekly or sub-weekly cadence.

Recent works have shown that the S-1 coherence can be used for parameter estimation [1] and land classification [2]. Most of previous works, however, have used simplified models of the temporal-volumetric coherence, or have treated the coherence as a feature in a machine learning or regression scheme. Here, we propose a three-stage procedure based on physical models, the *random-motion-over-ground* (RMoG) [3] and *water cloud* (WC) [4] models, to estimate tree height and other land parameters embedded in these models. The algorithm takes as main input time series of temporal SAR coherence and backscatter, as well as sparse lidar data to constrain the inverse problem.

The S-1 coherence and backscatter data set published in [5] and GEDI L2 data are used to assess the parameter estimation. While results with S-1 are promising, the algorithm will likely yield better results with low-frequency missions that are more robust to temporal decorrelation. The physical models are described in Section II; the data sets are described in Section III; the algorithm is presented in Section IV; and the S-1 results and their assessment with GEDI data are discussed in Section V.

II. Physical Models

A time series of temporal coherence over land can be modeled by the extended RMoG model that incorporates the decorrelation caused by motion of the scatterers and by changes in canopy and soil backscatter intensity between two interferometric SAR acquisitions [6], [7]. Given two SAR samples acquired at epochs t_1 and t_2, the expression of the RMoG temporal coherence model is

$$\gamma(t_1,t_2)=\frac{\sqrt{\mu_1\mu_2}\;\gamma_g+\gamma_v}{\sqrt{(\mu_1+1)(\mu_2+1)}} \tag{1}$$

where μ_1 and μ_2 are the ground-to-volume scattering ratios that differ due to dielectric changes between t_1 and t_2, and γ_g and γ_v are the ground-level (g) and vegetation (v) coherences [3], respectively,

$$\gamma_g=\exp\left[-\frac{1}{2}\left(\frac{4\pi}{\lambda}\right)^2\delta_g^2T\right],\quad \gamma_v=\gamma_g\frac{p(e^{qh}-1)}{q(e^{ph}-1)} \tag{2}$$

$$p=\frac{2\kappa}{\cos\theta},\quad q=p-\frac{1}{2}\left(\frac{4\pi}{\lambda}\right)^2\frac{\delta_v^2-\delta_g^2}{h_r}T \tag{3}$$

where $T=|t_2-t_1|$ is the temporal gap between the two SAR acquisitions, h is the vegetation height, $\kappa(t)$ is the average one-way attenuation coefficient of the vegetation, $\kappa=[\kappa(t_1)+\kappa(t_2)]/2$, θ is the look angle, δ_v^2 and δ_g^2 are the ground and canopy motion rate variances along the radar line-of-sight, respectively, and h_r is a constant reference height for the vegetation motion rate. Note that the parameters $\kappa(t)$, $\mu_1(t)$, $\mu_2(t)$, $\delta_v^2(t)$, and $\delta_g^2(t)$ change between two SAR acquisitions. The time dependence of the RMoG coherence is modeled through T following the assumption of the Brownian motion of the scatterers [8]. The coherence model (1) with two different ground-to-volume ratios μ_1 and μ_2 has been obtained with a procedure similar to the one followed in [3] by assuming only soil backscatter changes and ignoring penetration in the soil with associated decorrelation and phase effects modeled for instance in [9].

Manuscript received 18 September 2022; revised 21 December 2022; accepted 19 January 2023. Date of publication 2 February 2023; date of current version 7 February 2023. *(Corresponding author: M. Lavalle.)*

M. Lavalle is with the NASA Jet Propulsion Laboratory, California Institute of Technology, Pasadena, CA 91109 USA (e-mail: marco.lavalle@jpl.nasa.gov).

C. Telli and N. Pierdicca are with the Department of Information Engineering, Electronics and Telecommunications, Sapienza University, 00185 Rome, Italy.

U. Khati is with the Department of Astronomy, Astrophysics and Space Engineering, IIT Indore, Indore 453552, India.

O. Cartus is with Gamma Remote Sensing, 3073 Gümligen, Switzerland.

J. Kellndorfer is with Earth Big Data, Woods Hole, MA 02543 USA.

Digital Object Identifier 10.1109/LGRS.2023.3239825

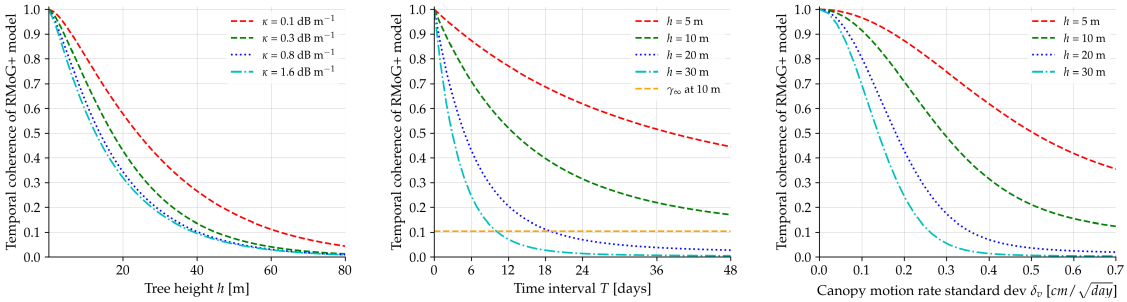

Fig. 1. Temporal C-band RMoG model coherence. Where applicable, fixed values are $\lambda = 5.6$ cm, $\theta = 37.55°$, $T = 6$ days, $\kappa = 0.3$ dB/m, $h = 10$ m, $\delta_g = 0$ m/$\sqrt{\text{day}}$, $\delta_v = 0.2$ cm/$\sqrt{\text{day}}$, $h_r = 10$ m, and $\mu_1 = \mu_2$. In the middle and right plots, μ varies between -6.4 and -27.7 dB.

The interferometric coherence $\gamma(t_1, t_2)$ can be linked to backscatter time series $\sigma(t)$ modeled by the WC model [4] by deriving the ground-to-volume ratio $\mu(t)$

$$\sigma(t) = \sigma_g(t)\, K(t) + \sigma_v(t)[1 - K(t)] \tag{4}$$

$$\mu(t) = \frac{\sigma_g(t)\, K(t)}{\sigma_v(t)[1 - K(t)]} = \frac{\sigma_g(t)}{\sigma_v(t)\left[e^{2\kappa(t)h/\cos\theta} - 1\right]} \tag{5}$$

where $\sigma_g(t)$ and $\sigma_v(t)$ are the time-varying soil and vegetation backscatter coefficients, respectively, and $K(t) = e^{-2\kappa(t)h/\cos\theta}$ is the time-varying transmission coefficient.

A. Model Sensitivity Analysis and Long-Term Coherence

Fig. 1 shows the C-band temporal coherence when backscatter changes are neglected ($\mu_1 = \mu_2$) and therefore the sensitivity of the coherence to tree height is caused only by differential motion ($\delta_v - \delta_g > 0$). Considering a 10-m-tall tree as an example, 0.2 cm/$\sqrt{\text{day}}$ canopy motion rate standard deviation, $\kappa = 0.3$ dB/m, the six-day coherence reduces up to 0.7. Due to the low penetration depth at shorter wavelengths, the C-band coherence compared to lower radar frequencies tends to be more sensitive to tree height when the vegetation is short, less dense, and sparse (i.e., with gaps). Both time interval and differential motion affect the coherence significantly, whereas the extinction coefficient has less impact, specially for κ values greater than 0.2 dB/m. At C-band, typical values of κ ranges between 0 and 2 dB/m [10], whereas δ_v can fluctuate between 0 and 1 cm/$\sqrt{\text{day}}$.

The RMoG model provides a physical interpretation for the long-term coherence γ_∞ included in existing semi-empirical coherence models (referred to as ρ_{LT} in [2] and ρ_∞ in [5]), $\gamma(t) = (1 - \gamma_\infty)e^{-t/\tau} + \gamma_\infty$, where τ is a time constant that controls the decay of the coherence over time t. When $\delta_g = 0$ m/$\sqrt{\text{day}}$ and $T \to \infty$, the RMoG model coherence becomes

$$\gamma_\infty = \frac{\sqrt{\mu_1 \mu_2}}{\sqrt{(\mu_1 + 1)(\mu_2 + 1)}}. \tag{6}$$

The value of γ_∞ is illustrated as a horizontal asymptote in Fig. 1. For long time intervals within a predefined time frame (e.g., a season), the coherence approaches a value that depends on the ground-to-volume scattering ratios evaluated within the time frame. Assuming temporal decorrelation caused only by scatterers motion ($\mu_1 = \mu_2$), a value of γ_∞ of 0.2 leads to a value of μ of about -6 dB. Smaller values of γ_∞ are associated with smaller values of μ because the ground is less visible to microwaves and the canopy layer decorrelates faster than the ground over long time intervals.

III. Description of the Dataset

A. S-1 Coherence and Backscatter Data

A recent effort funded by the NASA Jet Propulsion Laboratory generated a global backscatter and coherence data set from about 205 000 S-1 single-look-complex frames acquired between 1 December 2019, and 30 November 2020 [5]. Consistent six-day repeat coverage with about 60 image pairs from either ascending or descending orbits are available over Europe, the coastal areas of Greenland and Antarctica, and some smaller areas around the world. A consistent coverage with 12-day repeat-pass imagery, instead, can be observed almost globally. All coherence, backscatter, and supporting layers are available as GeoTIFF tiles to a fixed $1° \times 1°$ grid with a pixel spacing of three arcsecs. Coherence is calculated as the median across all co-polar coherence estimates of a given repeat interval (6, 12, 18, 24, 36, and 48) and from four seasonal three-month periods: 1) December/January/February; 2) March/April/May; 3) June/July/August; and 4) September/October/November. Coherence is estimated with a spatially adaptive multilooking window size to mitigate the estimation bias [5]. Backscatter is distributed as a seasonal average for the co- and cross-polar channels. The data set contains also γ_∞ and τ estimated by fitting an exponential decay model, $\gamma_t(t) = (1 - \gamma_\infty)e^{-t/\tau} + \gamma_\infty$ [2], to seasonal coherence samples with increasing repeat intervals. Fig. 2 shows the Fall S-1 coherence for six time intervals, backscatter, long-term coherence, and incidence angle for a region in Spain. Vegetation in our test site is dominated by Aleppo pine (*Pinus halepensis*) and Austrian pine (*Pinus nigra*), partially mixed with Scots pine (*Pinus sylvestris*) and oak (*Quercus ilex*). According to the ESA's CCI Biomass Map (2018, v3), the mean biomass is 41.90 Mg/ha with values up to 100 Mg/ha. Vegetation type is partly accounted for in (1) by κ and μ. Topographic variations are predominant for about half of the image, with local incidence angle varying mostly between 20° and 50°. Topography is modeled in (1) via μ.

B. Other Ancillary Data

Other data sets included in this study are the ESA World Cover Map (WCM), GEDI L2A/L3 data [11], and the global ecoregion map derived from the WWF ecoregion map. The 2021 ESA WCM is distributed as $3° \times 3°$ tiles, 2651 in total, 10-m resolution, and is based on both S-1 and S-2 data. Each tile is provided in EPSG:4326 projection and consists of two CO-GeoTIFF files, a land cover map with 11 classes

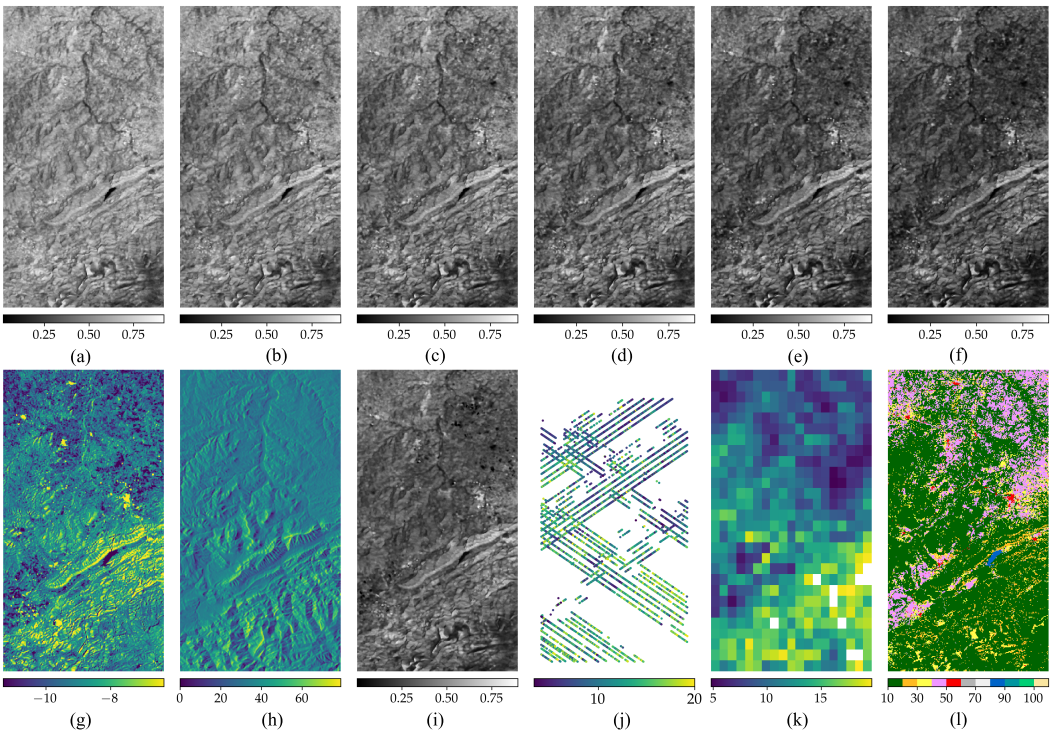

Fig. 2. S-1-derived layers [5], and GEDI and WCM data described in Section III for a region in Spain (lon: 0°–0.2°; lat: 40.7°–41°). This study includes the following WCM classes: trees (10), shrubs (20), grass (30), crops (40), and bare/sparse vegetation (60). (a) Fall COH 06 (-). (b) Fall COH 12 (-). (c) Fall COH 18 (-). (d) Fall COH 24 (-). (e) Fall COH 36 (-). (f) Fall COH 48 (-). (g) Backscatter σ_{VV} (dB). (h) Inc angle θ (°). (i) Fall γ_∞ (-). (j) GEDI L2A height (m). (k) GEDI L3 height (m). (l) ESA WCM.

and quality indicators of the S-1 and S-2 input data. The GEDI Level 3 gridded Land Surface Metrics [11] provides 15 data files in GeoTIFF format delivered in EPSG:6933 projection. Spatial resolution is 1 km, GEDI coverage is $+52°$, $-52°$ latitude, whereas temporal coverage is from 18 April 2019 to 4 August 2021. The GEDI L2A product contains elevation, RH100 canopy height and surface energy metrics extracted from reflected waveforms within each laser footprint, and it is sampled at 25-m resolution. In this study, all products are resampled to the S-1 data set resolution (3 arcsecs) using the Nearest Neighbor method, as shown in Fig. 2(j)–(l).

IV. Model-Based Retrieval Algorithm

The coherence model (1) contains three structural parameters (tree height h, mean extinction κ, and ground-to-volume scattering ratio μ_1) and three dynamic parameters causing temporal decorrelation (ground motion std-dev rate δ_g, canopy motion std-dev rate δ_v, and ground-to-volume scattering ratio μ_2) for a single coherence observation. Estimating all model parameters from multiple single-polarimetric coherence observations requires assumptions to avoid an ill-posed inverse problem. While it is difficult to select a priori values for the model parameters, we recommend the following strategy based on different assumptions and approaches tested with S-1 data. To reduce the number of model parameters, zero decorrelation due to soil/vegetation backscatter changes ($\mu_1 = \mu_2$) and zero ground-level motion ($\delta_g = 0$ m/$\sqrt{\text{day}}$) are assumed, which leaves h, κ, δ_v, and μ as unknown model parameters. While the assumption of zero ground-level temporal decorrelation may seem unrealistic, this decorrelation source is partially (and sub-optimally) accounted for by δ_v, which will then represent an aggregated motion-induced decorrelation parameter. Assuming $\mu_1 = \mu_2$ allows ground and vegetation backscatter coefficients to change by the same amount; in addition, a model analysis indicates a small level of decorrelation when $\mu_1 \neq \mu_2$. The idea for estimating these four parameters is to use sparse lidar data in conjunction with SAR coherence to estimate the spatially *slow*-varying model parameters (κ and δ_v), and then use coherence samples at multiple intervals to estimate the spatially *fast*-varying model parameters for each S-1 pixel (μ and h). The rationale behind choosing κ and δ_v as parameters that vary slowly across the image is that they are impacted to a large extent by weather conditions (e.g., rainfall, wind), which are expected to affect similarly adjacent pixels. The parameter estimation procedure can be broken into three stages as illustrated in Fig. 3.

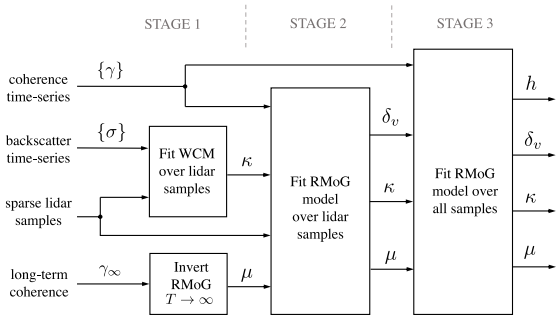

Fig. 3. Model-based estimation algorithm described in Section IV.

A. Three-Stage Parameter Estimation Algorithm

Parameter estimation (see Fig. 3) starts with the estimation of the ground-to-volume ratio μ for each coherence sample

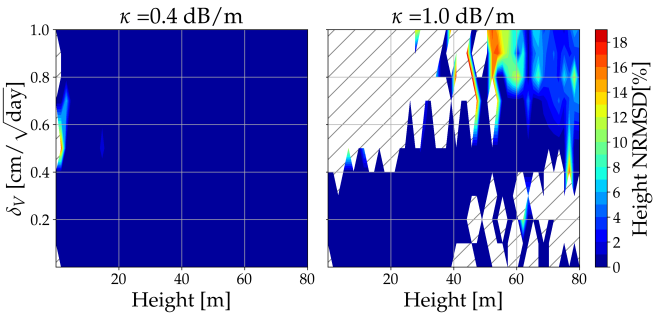

Fig. 4. Results of the estimation algorithm applied to model simulations. The striped pattern indicates unreliable tree height estimation (NRMSD > 20%) for the associated values of the input parameters.

via inversion of (6) (stage-1). The long-term coherence γ_∞ is considered as an input to the algorithm because it is already available in the coherence data set [5], but it can be estimated from the coherence time series as described in [5] if not available. The next step in stage-1 is the estimation of the spatially constant extinction coefficient κ (as well as σ_g and σ_v, which can be ignored) by fitting the WC model using total backscatter and sparse footprint-level lidar samples. In stage-2, the RMoG model is fit to estimate δ_v using tree height from sparse lidar footprint-level data, coherence samples for all time intervals over the lidar footprints, and ground-to-volume ratio μ and fixed κ found in stage-1. Sparse and spatially slow-varying δ_v estimates are spatially interpolated across the study site or eco-region to generate a continuous map of δ_v. Finally, in stage-3 tree height h for each coherence sample is obtained by performing a second RMoG model fitting using as inputs the coherence time series, the spatially varying δ_v and μ calculated in stage-2 and stage-1, respectively, and the fixed extinction coefficient κ calculated in stage-1. The algorithm can be applied separately within each eco-region or land-cover class as the values of the spatially constant κ parameter may change depending on land cover and vegetation characteristics.

B. Estimation Performance Assessment With Simulated Data

Prior to working with real data, the simplified model inversion was tested with RMoG model simulations to verify the correct algorithm implementation and assess the performance of the inversion algorithm independently of error sources. Simulated data were generated with tree height ranging from 0 to 80 m, δ_v ranging from 0 to 1 cm/$\sqrt{\text{day}}$, κ ranging from 0 to 2 dB/m, and μ fixed at -8 dB. Ten simulations for each set of parameters were conducted, and the result of the fitting was statistically analyzed across the simulation set to calculate the estimation performance. Fig. 4 shows the normalized rms difference (NRMSD) computed between input and estimated tree height for κ equal 0.4 and 1.4 dB/m. A threshold on the NRMSD (<20%) is applied to establish a validity range of values for the RMoG parameters that lead to correct model inversion. The analysis revealed that height estimation is always achievable for very small values of extinction coefficient (less than 0.4 dB/m), and it worsens for increasing κ and δ_v values. When κ approaches 1 dB/m, height retrieval is reliable for δ_v less than 0.3 cm/$\sqrt{\text{day}}$ and height values less than 40 m. Although not shown here, the other model parameters were estimated with similar performance.

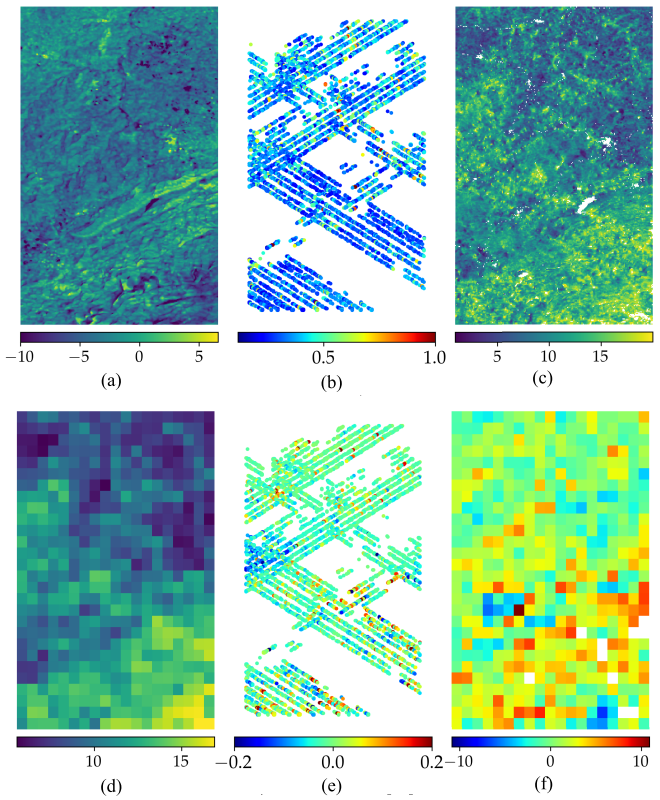

Fig. 5. Results of the model-based parameter estimation procedure of Fig. 3 applied to S-1 and GEDI data shown in Fig. 2. Size of GEDI samples is exaggerated for visualization purposes. (a) μ (dB). (b) δ_V (cm/$\sqrt{\text{day}}$). (c) h (m) (90 m). (d) h (m) (1 km). (e) GEDI L2A-h (m). (f) GEDI L3-h (m).

V. Application to S-1 Data

The algorithm of Fig. 3 was applied to S-1 coherence and backscatter data distributed in [5]. We selected a site in Spain (lon: 0°–0.2°; lat: 40.7°–41°) characterized by a Mediterranean biome with prevalence of tree cover class (79.5%). Trees are about 10 m high according to GEDI L2 data, with a standard deviation of 3.5 m and ranging between 0 and 20 m. Data in the Fall season were chosen because coherence appeared to be higher than the other seasons.

Fig. 5(a)–(c) shows the output μ, δ_v, and h of the algorithm applied to the input data of Fig. 2. The ground-to-volume ratio in Fig. 5(a) was derived by inverting (6) using γ_∞ of Fig. 2(i). As expected, μ reveals spatial heterogeneity linked to the land cover and vegetation characteristics, as well as terrain slope. This can be seen by comparing μ with Fig. 2(h) and (l). In the second step of stage-1 of the algorithm, the WC model is fit to backscatter data binned according to GEDI L2 canopy height sampled at 1 m intervals. The results of the WC model fitting are shown in Fig. 6. The extinction coefficients were found equal to $\kappa = 0.34$ and 0.35 dB/m for the VV and VH polarizations, respectively.

In stage-2, δ_v was estimated from the RMoG model fitting over the GEDI locations. The results are shown in Fig. 5(b). The map of sparse δ_v samples shows values ranging between 0 and 0.5 cm$\sqrt{\text{day}}$, for which the estimation algorithm is expected to perform well according to our simulations of Fig. 4 and given the value of $\kappa = 0.35$ dB/m. In stage-3, the S-1 coherence time series (six maps; samples with coherence less than 0.3 are ignored), μ, κ, and the spatially interpolated map

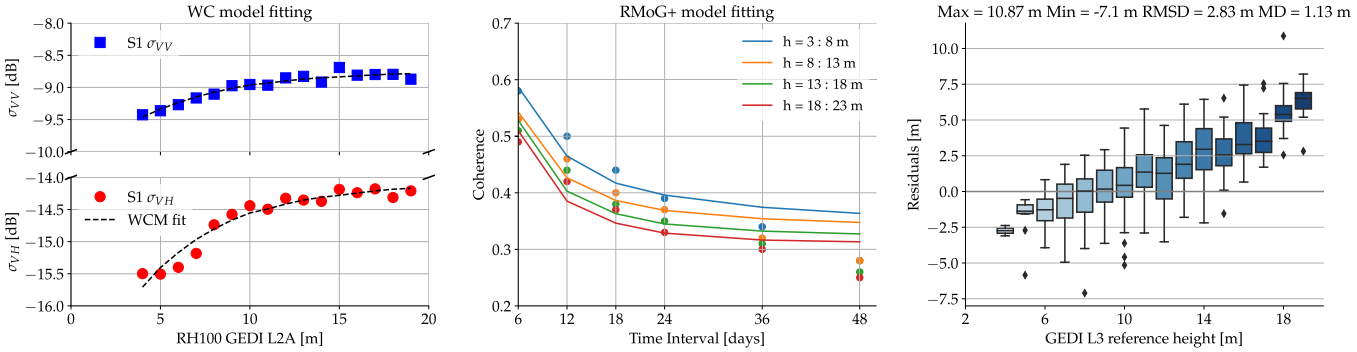

Fig. 6. WC model fit (left), S-1 Fall coherence with RMoG model fit (middle), and residuals of h estimated from S-1 (right).

of δ_v were given as inputs to the RMoG model fitting to estimate h. The results are shown in Fig. 5(c) and (d) for 90-m and 1-km posting, respectively. The middle plot in Fig. 6 illustrates the quality of the stage-3 model fitting as a function of the S-1 time gap and for increasing GEDI height intervals. Dots are the median coherences for a given time interval further averaged within increasing GEDI height ranges. Dashed lines show the RMoG model fit. The overestimation of coherence for long repeat intervals is likely due to the way κ and μ are estimated, in addition to possible bias in the estimation of δ_v.

Fig. 5(e) and (f) shows the difference between GEDI L2 data and h, and GEDI L3 data and h, respectively. While h matches the GEDI L2 height with sub-meter accuracy, the difference between GEDI L3 height and h appears small in the upper portion of the image and larger toward the bottom of the image where severe topography and taller trees occur. This spatial pattern of the error can also be ascribed to inaccuracies in the δ_v interpolation method and to the low resolution of the GEDI L3 map. The comparison of the S-1-derived tree height against the GEDI L3 canopy top height map reveals a general acceptable agreement with residuals stratified by canopy height shown in Fig. 6 (bottom). As a consequence of the slight mismatch between modeled and observed coherence, trees taller than 10–15 m tend to be underestimated whereas sparse/short vegetation is overestimated with respect to GEDI L3 data assumed here as a reference. The average RMSD of the estimated h is 2.83 m with a mean difference of 1.13 m.

VI. Conclusion

Estimating land parameters, such as tree height, from coherence time series is relevant to SAR missions like NISAR and ROSE-L that will generate global and dense time series of interferometric temporal coherence at L-band. This letter emphasizes the use of physical models that could complement or enhance alternative approaches based on machine learning or statistical regression. Results from S-1 data are promising, although a full assessment would require a global analysis. Several refinements can be devised to improve parameter retrieval, e.g., by relaxing some of the model assumptions, or by adopting a multiseasonal approach. We used the median seasonal coherence distributed in [5], but using the coherence that minimizes temporal decorrelation while maximizing the coherence contrast in the time series will likely yield better results. Also, changes in μ and ground-level decorrelation have been ignored causing δ_v to likely absorb partially or sub-optimally these decorrelation sources. More model parameters may be estimated by incorporating additional data sets such as moisture maps and wind measurements from other sensors.

Acknowledgment

This research was conducted at the Jet Propulsion Laboratory, California Institute of Technology, Pasadena, CA, USA, under contract with the National Aeronautics and Space Administration. All rights reserved. Government sponsorship acknowledged.

References

[1] O. Cartus, M. Santoro, U. Wegmuller, N. Labriere, and J. Chave, "Sentinel-1 coherence for mapping above-ground biomass in semiarid forest areas," *IEEE Geosci. Remote Sens. Lett.*, vol. 19, pp. 1–5, 2022.

[2] F. Sica, A. Pulella, M. Nannini, M. Pinheiro, and P. Rizzoli, "Repeat-pass SAR interferometry for land cover classification: A methodology using Sentinel-1 short-time-series," *Remote Sens. Environ.*, vol. 232, Oct. 2019, Art. no. 111277.

[3] M. Lavalle, M. Simard, and S. Hensley, "A temporal decorrelation model for polarimetric radar interferometers," *IEEE Trans. Geosci. Remote Sens.*, vol. 50, no. 7, pp. 2880–2888, Jul. 2012.

[4] M. Santoro, J. I. H. Askne, G. Smith, and J. E. S. Fransson, "Stem volume retrieval in boreal forests from ERS-1/2 interferometry," *Remote Sens. Environ.*, vol. 81, no. 1, pp. 19–35, 2002.

[5] J. Kellndorfer et al., "Global seasonal Sentinel-1 interferometric coherence and backscatter data set," *Sci. Data*, vol. 9, no. 1, pp. 1–16, Mar. 2022.

[6] M. Lavalle, "Soil moisture under vegetation: PolInSAR modeling, simulations and observations," in *Proc. PolInSAR Workshop*, Frascati, Italy, Jan. 2015, p. 16.

[7] M. Lavalle, U. Khati, G. H. X. Shiroma, and B. Chapman, "Assessment of PolSAR and InSAR time-series from the 2019 NASA AM-PM campaign for above-ground biomass estimation," in *Proc. IEEE Int. Geosci. Remote Sens. Symp.*, Sep. 2020, pp. 3861–3864.

[8] F. Lombardini and H. Griffiths, "Effect of temporal decorrelation on 3D SAR imaging using multiple pass beamforming," in *Proc. IEE-EUREL Meeting Radar Sonar Signal Process.*, Peebles, U.K., Jul. 1998, p. 34.

[9] F. De Zan, A. Parizzi, P. Prats-Iraola, and P. López-Dekker, "A SAR interferometric model for soil moisture," *IEEE Trans. Geosci. Remote Sens.*, vol. 52, no. 1, pp. 418–425, Jan. 2014.

[10] J. D. Ballester-Berman, "Reviewing the role of the extinction coefficient in radar remote sensing," 2020, *arXiv:2012.02609*.

[11] R. O. Dubayah, S. B. Luthcke, T. J. Sabaka, J. B. Nicholas, S. Preaux, and M. A. Hofton, "GEDI L3 gridded land surface metrics, version 1," ORNL DAAC, Oak Ridge, TN, USA, 2021.